Evaluation of ^{11}C-LSN3172176 as a Novel PET Tracer for Imaging M_1 Muscarinic Acetylcholine Receptors in Nonhuman Primates

Nabeel B. Nabulsi[1], Daniel Holden[1], Ming-Qiang Zheng[1], Frederic Bois[1], Shu-Fei Lin[1], Soheila Najafzadeh[1], Hong Gao[1], Jim Ropchan[1], Teresa Lara-Jaime[1], David Labaree[1], Anupama Shirali[1], Lawrence Slieker[2], Cynthia Jesudason[2], Vanessa Barth[2], Antonio Navarro[2], Nancy Kant[2], Richard E. Carson[1], and Yiyun Huang[1]

[1]*Yale PET Center, Department of Radiology and Biomedical Imaging, Yale University, New Haven, CT; and* [2]*Eli Lilly and Co., Indianapolis, Indiana*

The M_1 muscarinic acetylcholine receptor (mAChR) plays an important role in learning and memory, and therefore is a target for development of drugs for treatment of cognitive impairments in Alzheimer disease and schizophrenia. The availability of M_1-selective radiotracers for PET will help in developing therapeutic agents by providing an imaging tool for assessment of drug dose-receptor occupancy relationship. Here we report the synthesis and evaluation of ^{11}C-LSN3172176 (ethyl 4-(6-(methyl-^{11}*C*)-2-oxoindolin-1-yl)-[1,4'-bipiperidine]-1'-carboxylate) in nonhuman primates. **Methods:** ^{11}C-LSN3172176 was radiolabeled via the Suzuki–Miyaura cross-coupling method. PET scans in rhesus macaques were acquired for 2 h with arterial blood sampling and metabolite analysis to measure the input function. Blocking scans with scopolamine (50 μg/kg) and the M_1-selective agent AZD6088 (0.67 and 2 mg/kg) were obtained to assess tracer binding specificity and selectivity. Regional brain time–activity curves were analyzed with the 1-tissue-compartment model and the multilinear analysis method (MA1) to calculate regional distribution volume. Nondisplaceable binding potential values were calculated using the cerebellum as a reference region. **Results:** ^{11}C-LSN3172176 was synthesized with greater than 99% radiochemical purity and high molar activity. In rhesus monkeys, ^{11}C-LSN3172176 metabolized rapidly (29% ± 6% parent remaining at 15 min) and displayed fast kinetics and extremely high uptake in the brain. Imaging data were modeled well with the 1-tissue-compartment model and MA1 methods. MA1-derived distribution volume values were high (range, 10–81 mL/cm^3) in all known M_1 mAChR–rich brain regions. Pretreatment with scopolamine and AZD6088 significantly reduced the brain uptake of ^{11}C-LSN3172176, thus demonstrating its binding specificity and selectivity in vivo. The cerebellum appeared to be a suitable reference region for derivation of nondisplaceable binding potential, which ranged from 2.42 in the globus pallidus to 8.48 in the nucleus accumbens. **Conclusion:** ^{11}C-LSN3172176 exhibits excellent in vivo binding and imaging characteristics in nonhuman primates and appears to be the first appropriate radiotracer for PET imaging of human M_1 AChR.

Key Words: muscarinic; M_1 AChR; PET; radioligand; ^{11}C-LSN3172176; non-human primates; scopolamine

J Nucl Med 2019; 60:1147–1153
DOI: 10.2967/jnumed.118.222034

The muscarinic acetylcholine receptors (mAChRs) are G protein–coupled receptors widely expressed in the central nervous system, where they mediate acetylcholine neurotransmission (*1*) and thus are targets for drug discovery (*2*). Five main subtypes of mAChRs (M_1–M_5) have been identified. The M_1 receptor is abundantly expressed throughout the striatum, cortex, hippocampus, and amygdala (*3–6*). These regions are important for learning and memory and develop amyloid plaques in Alzheimer disease patients (*7*). Many studies showed that M_1-knockout mice display cognitive deficits (*3,8–10*), and activation of the M_1 mAChR had precognitive effects (*8,11–13*), improving memory and modulating hippocampal synaptic plasticity (*13–20*).

Given the important roles of M_1 mAChR in regulating memory, cognition, and behavior, selective M_1 activation has emerged as a potential treatment strategy for cognitive impairments in Alzheimer disease and schizophrenia (*21–24*). Therapeutic application of nonselective mAChR agonists, for example, melameline, sabcomeline, and xanomeline, has been limited by cholinergic adverse events such as diarrhea, nausea, gastrointestinal anomalies, salivation, and sweating thought to be mediated by mAChR subtypes other than M_1 (*25*). Therefore, there remains a need for developing M_1-selective drugs for potential treatment of cognitive disorders.

PET ligands that selectively bind to a target would greatly facilitate discovery of drugs with minimal to no side effects for superior therapeutic applications. Several PET ligands with affinity to M_1 have been reported, for example, ^{11}C-scopolamine (*26*), ^{11}C-NMPB (*27*), *N*-methyl ^{11}C-benztropine (*28*), and ^{11}C-QNB (*29*) (Fig. 1). These ligands have good brain uptake and were used to map mAChR in primate brains. However, they lack M_1 selectivity and display slow or irreversible binding kinetics. ^{11}C-xanomeline and the M_1 allosteric agonist ^{11}C-GSK-1034702 are among the available nonselective agonist PET ligands exhibiting limited specific binding despite clear brain penetration (*30,31*). ^{11}C-AF150(S) was recently reported as an agonist PET ligand for M_1 receptors

Received Oct. 17, 2018; revision accepted Dec. 29, 2018.
For correspondence or reprints contact: Nabeel B. Nabulsi, Yale PET Center, P.O. Box 208048, Yale School of Medicine, New Haven, CT 06520.
E-mail: nabeel.nabulsi@yale.edu
Published online Feb. 7, 2019.

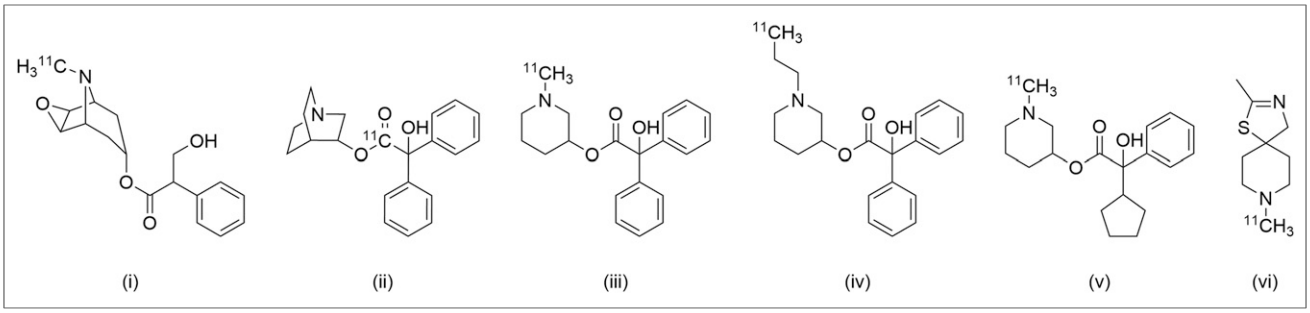

FIGURE 1. Chemical structures of selected PET radioligands for mAChRs: (i) ^{11}C-scopolamine; (ii) ^{11}C-QNB; (III) ^{11}C-MPB; (iv) ^{11}C-PPB; (v) (*S*)-1-(methyl-^{11}C)piperidin-3-yl (*R*)-2-cyclopentyl-2-hydroxy-2-phenylacetate; (vi) ^{11}C-AF150(S).

and evaluated in rats (*32,33*). However, the authors concluded that its use in brain imaging would be challenging due to its low lipophilicity (log D of 0.050), rapid metabolism, and moderate affinity (K_d of 200 nM for M_1 in rat cerebral cortex) (*32*). More recently, (*S*)-1-(methyl-^{11}*C*)piperidin-3-yl (*R*)-2-cyclopentyl-2-hydroxy-2-phenylacetate was reported as a high-affinity (K_i = 3.5 nM) radioligand based on the chemical scaffold of the antagonist MPB, but it appears to possess limited in vivo binding specificity, as its uptake was only partially blocked by the M_1-selective antagonist pirenzepine (*34*).

We recently reported the discovery of two novel M_1 mAChR-selective agonist ligands, LSN3172176 and LSN3262527 (Fig. 2), which are amenable to ^{11}C-radiolabeling (*35,36*). Here we report the radiosynthesis of ^{11}C-LSN3172176 (ethyl 4-(6-(methyl-^{11}*C*)-2-oxoindolin-1-yl)-[1,4'-bipiperidine]-1'-carboxylate) and its in vivo characterization in nonhuman primates.

MATERIALS AND METHODS

Both the reference standard LSN3172176 and the boronic acid precursor LSN3234794 were prepared by Eli Lilly & Co. (Lilly Research Centre) according to published procedures (*37*). Figure 3 outlines brief synthetic schemes for LSN3172176 and LSN3234794, including radiosynthesis of ^{11}C-LSN3172176 (the supplemental materials provide more details; supplemental materials are available at http://jnm.snmjournals.org).

In Vitro and In Vivo Properties

All in vitro pharmacologic characterization and in vivo validation of LSN3172176 as an M_1-selective mAChR PET tracer candidate were described recently (*38*). EC_{50} (half the maximal effective concentration that induces a response) values were 7.0, 3.7, and 2.4 nM in mouse, rat, and human, respectively. Binding affinity (K_i, nM) for mAChRs was in the following rank order: M_1 (8.9) > > M_4 (41.4) > M_5 (55.6), M_2 (63.8) > M_3 (3,031).

PET Imaging Experiments in Rhesus Monkeys

General PET Study Design. Imaging experiments were performed in rhesus monkeys (*Macaca mulatta*) according to a protocol approved by the Yale University Institutional Animal Care and Use Committee. Two sets of scans were obtained: a baseline scan with ^{11}C-LSN3172176 followed by a blocking scan after administration of scopolamine (50 μg/kg) over 10 min at about 40 min before the start of the second scan (n = 2); and 2 blocking scans with ^{11}C-LSN3172176 after pretreatment with the known M_1-selective partial agonist AZD6088 at the doses of 0.67 and 2 mg/kg, both given over 15 min at about 2 h before the injection of ^{11}C-LSN3172176.

PET Scan and Image Analysis Procedures. Subjects were sedated approximately 2 h before the first PET scan and kept anesthetized for the duration of the experiments as previously described (*39*).

Brain images were acquired using the FOCUS 220 PET scanner (Siemens Preclinical Solutions) with a reconstructed image resolution of about 1.5 mm. After a transmission scan, ^{11}C-LSN3172176 was injected intravenously over 3 min using an infusion pump as reported previously (*39*). List-mode data were acquired for 120 min and binned into sinograms with the following frame timing: 6 × 30 s, 3 × 1 min, 2 × 2 min, and 22 × 5 min.

Scan data were reconstructed with a Fourier rebinning/filtered backprojection algorithm as described previously (*39*). Regions of interest (n = 16) were previously delineated on a single representative anatomic rhesus monkey MR image registered to a template image. Regions used in this study were the amygdala, brain stem, caudate, cerebellum, cingulate cortex, frontal cortex, globus pallidus, hippocampus, insula, nucleus accumbens, occipital cortex, pons, putamen, substantia nigra, temporal cortex, and thalamus. Registration parameters (from PET-to-MR and from MR-to-atlas) were obtained to apply the regions of interest to individual PET scans (*40*), and regional time–activity curves were generated and expressed in SUV by normalizing by the injected dose and animal body weight.

Metabolite Analysis, Arterial Input Function, and Log D *Determination.* Arterial blood samples were collected to determine the unmetabolized parent fraction using the automatic column-switching high-performance liquid chromatography system (*41*) and to calculate the plasma input function. The plasma free fraction (f_p) was measured in triplicate using the ultrafiltration method, and the log *D* was determined by modification of the previously published procedure (*42*). Additional details are provided in the supplemental materials.

Data Analysis. Regional brain time–activity curves were analyzed with the 1-tissue-compartment (1T) model. Fit quality was compared with the 2-tissue-compartment model and the multilinear analysis-1 (MA1) method (*43*) to calculate the distribution volume (V_T). In MA1, data were fitted starting at time t^* = 30 min. Regional nondisplaceable binding potential (BP_{ND}) values were calculated using MA1 V_T values with the cerebellum as the reference region (*44*). The simplified

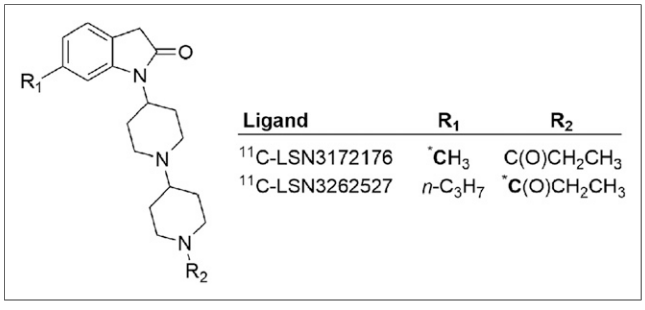

FIGURE 2. Novel selective agonist for M_1 mAChR. Boldface letter C with asterisk indicates ^{11}C-radiolabeling site.

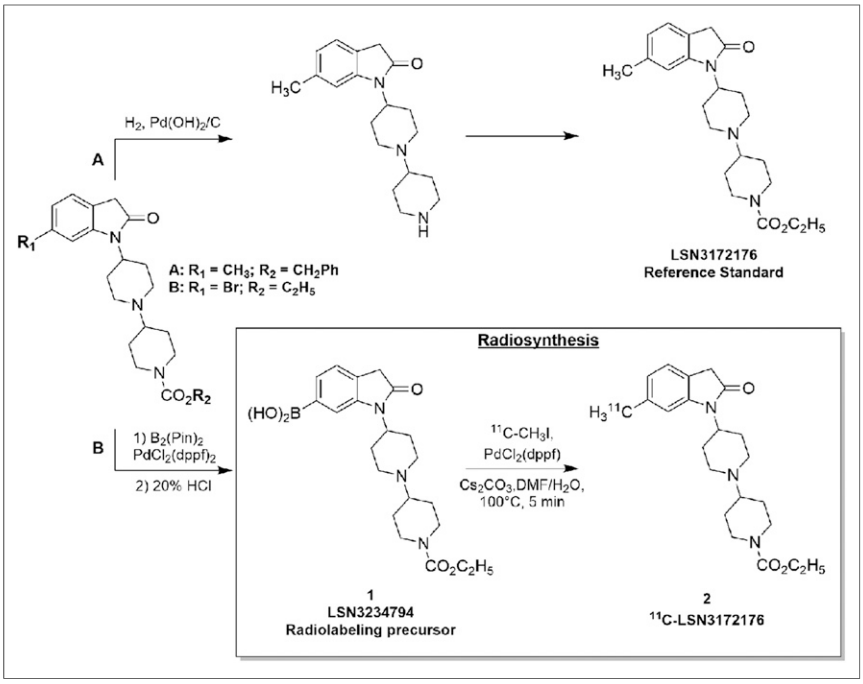

FIGURE 3. Brief scheme outlining synthesis of LSN3172176 and radiolabeling precursor, as well as radiosynthesis of ^{11}C-LSN3172176.

reference tissue model (SRTM) (*45*) was also used to calculate regional BP_{ND} values with the cerebellum as the reference region.

For the blocking experiments, target occupancy was estimated using the Lassen plot approach, which can determine the nondisplaceable volume of distribution (V_{ND}) and receptor occupancy using V_T values at baseline and after pretreatment (*46*).

RESULTS

Radiochemistry

^{11}C-LSN3172176 was synthesized via Pd^0-mediated cross-coupling of ^{11}C-iodomethane (*47*) with 1–1.2 mg of the boronic acid precursor (*48,49*) in 49.3% ± 16.6% radiochemical yield (decay-corrected) at the end of beam based on trapped ^{11}C-iodomethane radioactivity (n = 12). The radiochemical purity was greater than 99%, and the average molar activity (A_m) was 422 ± 259 MBq/nmol at the end of synthesis. Total synthesis time was 47 ± 5 min from the end of beam. The radiochemical purity remained greater than 98% at 60 min after the end of synthesis. The supplemental materials provide details.

PET Scans in Rhesus Monkeys

The mean injected dose of ^{11}C-LSN3172176 was 187 ± 3 MBq, with an A_m of 225 ± 100 MBq/nmol at the time of injection, and injected mass was 0.041 ± 0.018 μg/kg.

Plasma Analysis. Parent fraction and radioactivity in plasma over time are presented in Figure 4. ^{11}C-LSN3172176 metabolized rapidly. The parent fraction accounted for 29% ± 6% of the radioactivity at 15 min after injection, which decreased to 10% ± 3% at 90 min (n = 8). All radiometabolites were more polar than the parent compound (Supplemental Fig. 1: retention times ~3 and 7 min, compared with ~11 min for the parent). The f_p was high, at 41% ± 3% (n = 12). The measured log D of ^{11}C-LSN3172176 was 2.96 ± 0.02, in the optimal range (1–3.5) for brain PET radiotracers (*50*).

Image Analysis and Kinetic Modeling. Representative brain PET images summed from 30 to 45 min after tracer injection are shown in Figure 5. At baseline, high uptake was seen throughout the brain (Fig. 5A), with SUV highest in the striatum followed by cortical regions, and lowest in the cerebellum. Pretreatment with the nonselective mAChR antagonist scopolamine (50 μg/kg) markedly decreased radioactivity uptake (Fig. 5B), confirming in vivo binding specificity of ^{11}C-LSN3172176. Likewise, blockade by the M_1-selective partial agonist AZD6088 (2 mg/kg) confirmed ^{11}C-LSN3172176 in vivo selectivity for M_1 mAChR (Fig. 5C).

Regional brain time–activity curves are presented in Figure 6. ^{11}C-LSN3172176 displayed high uptake and reversible kinetics, with an SUV_{peak} of 4–9.5 and peak uptake time ranging from 10 to 50 min after administration (Fig. 6A). Pretreatment with 50 μg of scopolamine per kilogram reduced uptake across all regions to levels similar to that in the cerebellum, with regional radioactivity peaking earlier and clearing faster (Fig. 6B). Similarly, pretreatment with AZD6088 (2 mg/kg) reduced uptake in all brain regions to more homogeneous levels, demonstrating target selectivity (Fig. 6C).

It is known that the cerebellum is almost devoid of mAChRs (*51,52*). Indeed, uptake in the cerebellum did not change significantly between baseline and scopolamine-blocking scans (Fig. 6B), supporting the use of the cerebellum as the reference region.

The 1T model produced suitable but less than ideal fits of regional time–activity curves. MA1 (t^* = 30) produced good fits and stable estimates of V_T values well correlated with those from 1T (Supplemental Fig. 2). Overall, the 2-tissue-compartment model did not provide reliable V_T values, with most of the estimates having SEs of greater than 25% (data not shown). Thus, MA1 was chosen for analysis.

Table 1 presents regional V_T values derived from MA1. V_T values are higher in the striatal (putamen, nucleus accumbens,

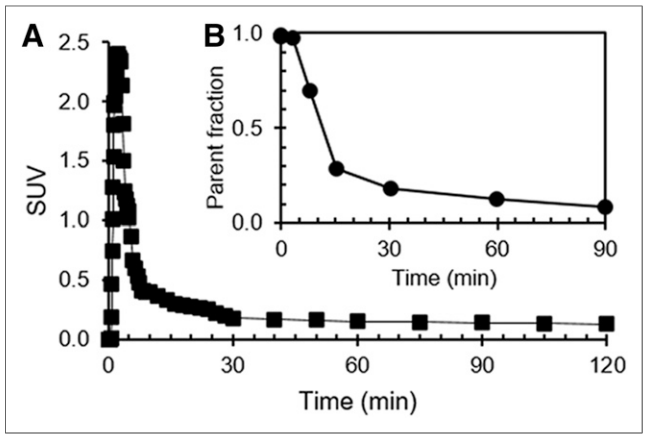

FIGURE 4. Metabolite-corrected plasma activity (A) and parent fraction in plasma (B) over time for ^{11}C-LSN3172176.

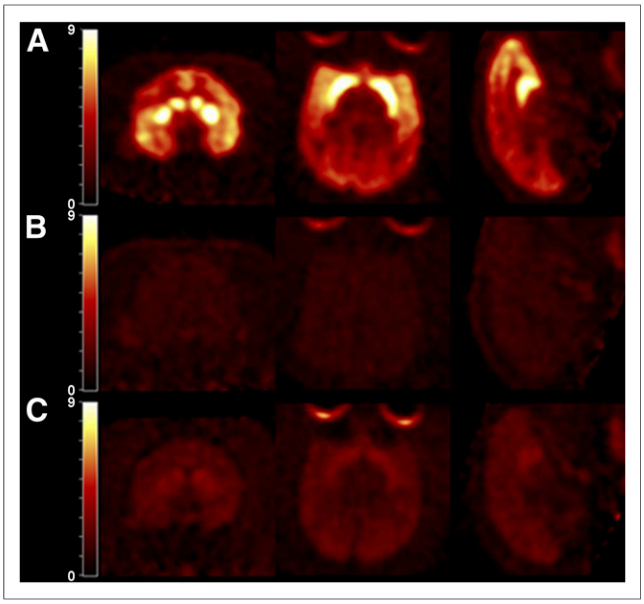

FIGURE 5. Representative PET SUV images summed from 30 to 45 min after ^{11}C-LSN3172176 injection from baseline scan (A), after pretreatment with scopolamine (50 μg/kg) (B), and after pretreatment with AZD6088 (2 mg/kg) (C).

and caudate) and cortical areas; moderate in the hippocampus, amygdala, and globus pallidus; and lower in other regions. Dramatic reduction in regional V_T was seen with administration of scopolamine (50 μg/kg). Likewise, preblocking with 2 doses of AZD6088 resulted in a clear and dose-dependent reduction in regional V_T. Regions with low V_T estimates (pons, brain stem, and cerebellum) displayed negligible changes. The average receptor occupancy calculated from the occupancy plot was 98.6% by 50 μg of scopolamine per kilogram (Fig. 7). Occupancies of 68% and 89% were found with 0.67 and 2 mg/kg of AZD6088, respectively. The average V_{ND} in the blocking scans with scopolamine and with the 2 doses of AZD6088 was calculated to be 6.3 ± 0.8 mL/cm^3.

Regional BP_{ND} values were calculated from the MA1 V_T values using the cerebellum as the reference region (Table 1). Note that the average V_{ND} value of 6.3 ± 0.8 mL/cm^3 estimated from the blocking scans is in good agreement with the mean baseline V_T value of 8.1 ± 1.3 mL/cm^3 for the cerebellum, indicating the cerebellum may be a suitable reference region. In vitro studies showed no significant ^{3}H-LSN3172176 binding to the cerebellum in monkey tissue and across other species (*38*). The minimal reduction in cerebellum V_T caused by blockade may be due to partial-volume effects from the high uptake in gray matter regions.

Regional BP_{ND} values derived from the SRTM using the cerebellum as the reference region are also listed in Table 1. SRTM produced good fits of regional time–activity curves and reliable BP_{ND} estimates. The highest V_T and BP_{ND} observed in the nucleus accumbens are consistent with autoradiographic study of M_1 distribution in the human brain (*53*). In addition to the role of the nucleus accumbens in the reward circuit (*54*), it is reported to be important in spatial learning and memory as well (*55*). BP_{ND} values derived from the SRTM method were consistently lower by about 25% across all brain regions (Supplemental Fig. 3A). A scatterplot of SRTM and MA1 BP_{ND} (Supplemental Fig. 3B) for the same selected brain regions showed excellent correlation (r = 0.998), with slope of 0.746 and intercept close to zero (0.155). Lower SRTM-derived BP_{ND} values are not uncommon for many tracers, due to violation of SRTM assumptions (*56*).

The MA1-estimated BP_{ND} for the cortical tissue is noteworthy. The measured in vitro B_{max} and K_D for ^{3}H-LSN3172176 binding in rhesus cortex are 843 ± 69 fmol/mg of protein (843 ± 69 nM) and 8 ± 3 nM (n = 3), respectively (*38*), yielding an in vitro BP (=B_{max}/K_D) value of 105.4. The average V_{ND} calculated from all 4 blocking scans (2 with scopolamine and 2 with AZD6088) in this study was 6.3 ± 0.8 mL/cm^3, and f_p was 0.41 ± 0.03. As BP_{ND} = f_{ND}*B_{max}/K_D and f_{ND} = f_p/V_{ND} = 0.065, the in vitro BP_{ND} for rhesus cortex would be 6.86, which is in good agreement with the in vivo BP_{ND} values for the frontal (5.33), occipital (4.02), and temporal (5.01) cortices estimated with PET (Table 1).

DISCUSSION

We presented the synthesis and evaluation of a first M_1 mAChR-selective PET radiotracer, ^{11}C-LSN3172176. The ligand was discovered by Lilly (*35,38*) in ex vivo ligand binding assays

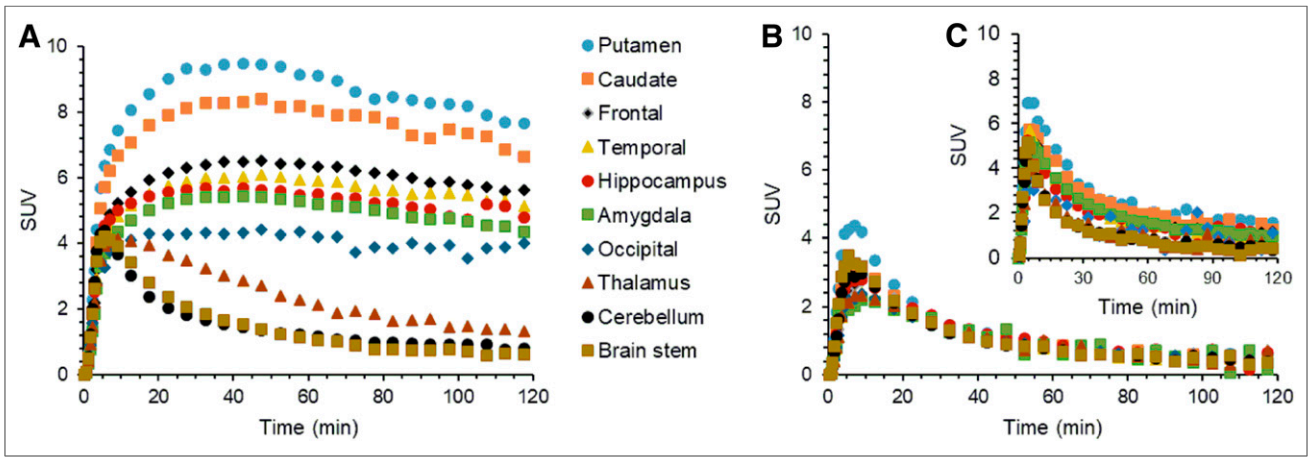

FIGURE 6. Representative time–activity curves in selected brain regions from ^{11}C-LSN3172176 baseline (A) and blocking scans after pretreatment with scopolamine (50 μg/kg) (B), and with 2 mg of AZD6088 (2 mg/kg) (C).

TABLE 1
Regional Binding Parameters for ^{11}C-LSN3172176 at Baseline and After Preblocking with Scopolamine and AZD6088

Brain region	Baseline V_T (n = 4)	Preblocking V_T (MA1, t^* = 30)			BP_{ND}	
			AZD6088			
		Scopolamine, 50 μg/kg (n = 2)	0.67 mg/kg (n = 1)	2 mg/kg (n = 1)	SRTM, baseline (n = 4)	MA1 (t^* = 30), baseline (n = 4)
Amygdala	33.8 (4.0)	7.2 (1.3)	13.49	8.40	2.54 (0.3)	3.23 (0.54)
Brain stem	7.7 (0.9)	7.3 (1.1)	7.28	5.99	0.08 (0.02)	−0.04 (0.07)
Caudate	62.6 (10)	8.0 (1.0)	24.29	13.83	5.46 (0.62)	6.77 (0.76)
Cerebellum	8.1 (1.3)	7.0 (1.2)	7.37	6.41	–	–
Cingulate	53.8 (7.1)	8.1 (0.8)	19.55	12.12	4.45 (0.2)	5.68 (0.26)
Frontal cortex	50.7 (5)	7.5 (0.5)	17.92	11.25	4.03 (0.2)	5.33 (0.37)
Globus pallidus	27.4 (2.6)	7.8 (1.3)	15.59	9.14	2.09 (0.14)	2.42 (0.21)
Hippocampus	43.5 (6.0)	8.0 (1.3)	18.16	10.19	3.37 (0.31)	4.41 (0.51)
Insula	56.6 (7.9)	7.8 (1.1)	18.50	11.65	4.56 (0.31)	6.02 (0.38)
Nucleus accumbens	75.6 (4.7)	8.2 (1.3)	30.33	12.82	6.24 (0.44)	8.48 (0.85)
Occipital cortex	40.4 (5.2)	7.1 (0.9)	18.11	11.54	3.08 (0.13)	4.02 (0.18)
Pons	8.5 (1.1)	8.1 (0.9)	8.26	7.06	0.17 (0.04)	0.05 (0.06)
Putamen	68.6 (10.7)	8.8 (2.0)	26.67	15.85	6.04 (0.59)	7.50 (0.6)
Substantia nigra	10.3 (1.8)	7.7 (1.3)	8.55	10.57	0.37 (0.05)	0.27 (0.07)
Temporal cortex	48.5 (6.9)	6.8 (0.7)	17.76	11.00	3.77 (0.18)	5.01 (0.22)
Thalamus	13.6 (1.7)	7.0 (1.1)	10.75	7.11	0.75 (0.12)	0.69 (0.14)

Values in parentheses are SDs.

using liquid chromatography–mass spectrometry (LC-MS/MS) (*57–59*). ^{11}C-LSN3172176 was reliably produced in good radiochemical yield, high radiochemical and chemical purity, and high molar activity, using the palladium catalyzed C-^{11}C Suzuki cross-coupling reaction (*49*) between ^{11}C-methyl iodide and the 2-oxoindolin-6-yl boronic acid precursor.

^{11}C-LSN3172176 displayed good pharmacokinetic and imaging characteristics in rhesus monkeys: high brain uptake, with an SUV_{peak} of 4–9.5 in the striatal and cortical tissues, and low uptake in the cerebellum, brain stem, and pons. Time–activity curves were well fitted by the MA1 (t^* = 30) to produce stable measures of regional V_T: highest in the basal ganglia, frontal cortex, and hippocampus, with low V_T in the cerebellum. PET images were of high quality, and tissue kinetics were suitable for an ^{11}C-labeled tracer, with high f_p that can be measured reliably. As predicted from in vitro binding experiments (*38*), uptake in the monkey brain was seen in all M_1 mAChR-rich brain regions similar to the known distribution reported for mouse, rat, and rhesus monkey (*3,26,60*). High specific binding was also reflected in the BP_{ND} estimates of 4–8.5. The specificity of ^{11}C-LSN3172176 binding to mAChRs was demonstrated by pretreatment with scopolamine, which reduced ^{11}C-LSN3172176 V_T values to levels indistinguishable from the cerebellum, resulting in 98.5% occupancy. Selectivity for M_1 mAChR was demonstrated by blocking of tracer uptake with the M_1-selective partial agonist AZD6088 in a dose-dependent manner, reducing V_T values across all brain regions to fairly homogeneous levels on preblocking with 2 mg/kg of AZD6088. The lowest V_T was found in the cerebellum and brain stem, with baseline V_T values of 8.1 and 7.7 mL/cm^3, respectively. The average V_{ND} value of 6.3 ± 0.8 mL/cm^3 derived from the blocking scans was in good agreement with the average baseline V_T in the cerebellum, indicating that the cerebellum may be suitable as a reference region for ^{11}C-LSN3172176. This is in line with previous reports that the cerebellum is devoid of mAChRs (*51,52*). The small difference in cerebellum between baseline and blocking scans is likely attributable to partial-volume averaging of cortical uptake into the cerebellum region in the baseline scan. To confirm this, we created a region of interest in the inferior portion of the cerebellum and measured the V_T values in control and blocking scans. In this inferior region, we found no difference between baseline V_T (6.3 ± 1.3) and postblocking V_T (6.8 ± 1.0) values, further supporting the utility of the cerebellum as a reference region.

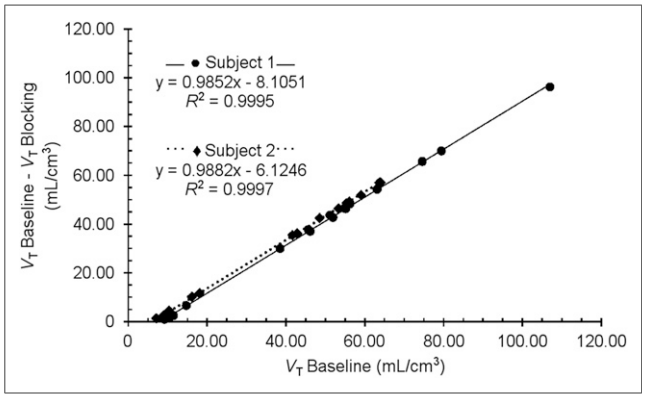

FIGURE 7. Occupancy plots for ^{11}C-LSN3172176 preblocking scans with scopolamine (50 μg/kg, n = 2).

CONCLUSION

We have performed the synthesis and preclinical evaluation of the novel M_1 mAChR-selective radioligand ^{11}C-LSN3172176 and demonstrated its suitability as a PET tracer for quantifying central M_1 mAChR in nonhuman primates. ^{11}C-LSN3172176 displays high levels of regional uptake and appropriate kinetics in rhesus monkey brain, as well as high regional specific binding signals. Therefore ^{11}C-LSN3172176 was advanced to human studies for further evaluation.

DISCLOSURE

Research support was provided by Eli Lilly and Co. At the time this work was conducted, Nancy Kant and Cynthia Jesudason were employees of Eli Lilly. No other potential conflict of interest relevant to this article was reported.

ACKNOWLEDGMENTS

We thank the staff of the Yale PET Center for their expert assistance.

REFERENCES

1. Thiele A. Muscarinic signaling in the brain. *Annu Rev Neurosci.* 2013;36:271–294.
2. Kruse AC, Kobilka BK, Gautam D, Sexton PM, Christopoulos A, Wess J. Muscarinic acetylcholine receptors: novel opportunities for drug development. *Nat Rev Drug Discov.* 2014;13:549–560.
3. Anagnostaras SG, Murphy GG, Hamilton SE, et al. Selective cognitive dysfunction in acetylcholine M1 muscarinic receptor mutant mice. *Nat Neurosci.* 2003;6: 51–58.
4. Levey AI. Muscarinic acetylcholine receptor expression in memory circuits: implications for treatment of Alzheimer disease. *Proc Natl Acad Sci USA.* 1996;93: 13541–13546.
5. Levey AI, Edmunds SM, Koliatsos V, Wiley RG, Heilman CJ. Expression of m1-m4 muscarinic acetylcholine receptor proteins in rat hippocampus and regulation by cholinergic innervation. *J Neurosci.* 1995;15:4077–4092.
6. Levey AI, Kitt CA, Simonds WF, Price DL, Brann MR. Identification and localization of muscarinic acetylcholine receptor proteins in brain with subtype-specific antibodies. *J Neurosci.* 1991;11:3218–3226.
7. Serrano-Pozo A, Frosch MP, Masliah E, Hyman BT. Neuropathological alterations in Alzheimer disease. *Cold Spring Harb Perspect Med.* 2011;1: a006189.
8. Wess J, Eglen RM, Gautam D. Muscarinic acetylcholine receptors: mutant mice provide new insights for drug development. *Nat Rev Drug Discov.* 2007; 6:721–733.
9. Wess J. Muscarinic acetylcholine receptor knockout mice: novel phenotypes and clinical implications. *Annu Rev Pharmacol Toxicol.* 2004;44:423–450.
10. Shinoe T, Matsui M, Taketo MM, Manabe T. Modulation of synaptic plasticity by physiological activation of M1 muscarinic acetylcholine receptors in the mouse hippocampus. *J Neurosci.* 2005;25:11194–11200.
11. Nathan PJ, Watson J, Lund J, et al. The potent M1 receptor allosteric agonist GSK1034702 improves episodic memory in humans in the nicotine abstinence model of cognitive dysfunction. *Int J Neuropsychopharmacol.* 2013;16:721–731.
12. van der Zee EA, Luiten PG. Muscarinic acetylcholine receptors in the hippocampus, neocortex and amygdala: a review of immunocytochemical localization in relation to learning and memory. *Prog Neurobiol.* 1999;58:409–471.
13. Foster DJ, Choi DL, Conn PJ, Rook JM. Activation of M1 and M4 muscarinic receptors as potential treatments for Alzheimer's disease and schizophrenia. *Neuropsychiatr Dis Treat.* 2014;10:183–191.
14. Lebois EP, Schroeder JP, Esparza TJ, et al. Disease-modifying effects of M1 muscarinic acetylcholine receptor activation in an Alzheimer's disease mouse model. *ACS Chem Neurosci.* 2017;8:1177–1187.
15. Ma L, Seager MA, Wittmann M, et al. Selective activation of the M1 muscarinic acetylcholine receptor achieved by allosteric potentiation. *Proc Natl Acad Sci USA.* 2009;106:15950–15955.
16. Jiang S, Li Y, Zhang C, et al. M1 muscarinic acetylcholine receptor in Alzheimer's disease. *Neurosci Bull.* 2014;30:295–307.
17. Scarr E. Muscarinic M1 receptor agonists: can they improve cognitive performance? *Int J Neuropsychopharmacol.* 2013;16:717–720.
18. Carruthers SP, Gurvich CT, Rossell SL. The muscarinic system, cognition and schizophrenia. *Neurosci Biobehav Rev.* 2015;55:393–402.
19. Hatcher JP, Loudon JM, Hagan JJ, Clark MS. Sabcomeline (SB-202026), a functionally selective M1 receptor partial agonist, reverses delay-induced deficits in the T-maze. *Psychopharmacology (Berl).* 1998;138:275–282.
20. Wienrich M, Meier D, Ensinger HA, et al. Pharmacodynamic profile of the M1 agonist talsaclidine in animals and man. *Life Sci.* 2001;68:2593–2600.
21. Caccamo A, Fisher A, LaFerla FM. M1 agonists as a potential disease-modifying therapy for Alzheimer's disease. *Curr Alzheimer Res.* 2009;6:112–117.
22. Sellin AK, Shad M, Tamminga C. Muscarinic agonists for the treatment of cognition in schizophrenia. *CNS Spectr.* 2008;13:985–996.
23. Fisher A. M1 muscarinic agonists target major hallmarks of Alzheimer's disease: an update. *Curr Alzheimer Res.* 2007;4:577–580.
24. Fisher A. M1 muscarinic agonists target major hallmarks of Alzheimer's disease: the pivotal role of brain M1 receptors. *Neurodegener Dis.* 2008;5:237–240.
25. Felder CC, Goldsmith PJ, Jackson K, et al. Current status of muscarinic M1 and M4 receptors as drug targets for neurodegenerative diseases. *Neuropharmacology.* 2018;136(pt. C):449–458.
26. Vora MM, Finn RD, Boothe TE, Liskwosky DR, Potter LT. [N-methyl-^{11}C]-scopolamine: synthesis and distribution in rat brain. *J Labelled Comp Radiopharm.* 1983;20:1229–1236.
27. Mulholland GK, Kilbourn MR, Sherman P, et al. Synthesis, in vivo biodistribution and dosimetry of [^{11}C]N-methylpiperidyl benzilate ([^{11}C]NMPB), a muscarinic acetylcholine receptor antagonist. *Nucl Med Biol.* 1995;22:13–17.
28. Dewey SL, Macgregor RR, Brodie JD, et al. Mapping muscarinic receptors in human and baboon brain using [N-^{11}C-methyl]-benztropine. *Synapse.* 1990;5:213–223.
29. Varastet M, Brouillet E, Chavoix C, et al. In vivo visualization of central muscarinic receptors using [^{11}C]quinuclidinyl benzilate and positron emission tomography in baboons. *Eur J Pharmacol.* 1992;213:275–284.
30. Farde L, Suhara T, Halldin C, et al. PET study of the M1-agonists [^{11}C]xanomeline and [^{11}C]butylthio-TZTP in monkey and man. *Dementia.* 1996;7:187–195.
31. Ridler K, Cunningham V, Huiban M, et al. An evaluation of the brain distribution of [^{11}C]GSK1034702, a muscarinic-1 (M 1) positive allosteric modulator in the living human brain using positron emission tomography. *EJNMMI Res.* 2014;4:66.
32. Buiter HJ, Windhorst AD, Huisman MC, et al. [^{11}C]AF150(S), an agonist PET ligand for M1 muscarinic acetylcholine receptors. *EJNMMI Res.* 2013;3:19.
33. Buiter HJC, Leysen JE, Schuit RC, Fisher A, Lammertsma AA, Windhorst AD. Radiosynthesis and biological evaluation of the M1 muscarinic acetylcholine receptor agonist ligand [^{11}C]AF150(S). *J Labelled Comp Radiopharm.* 2012;55:264–273.
34. Malmquist J, Varnas K, Svedberg M, et al. Discovery of a Novel Muscarinic Receptor PET Radioligand with Rapid Kinetics in the Monkey Brain. *ACS Chem Neurosci.* 2018;9:224–229.
35. Jesudason C, Barth V, Goldsmith P, et al. Discovery of two novel, selective agonist radioligands as PET imaging agents for the M1 muscarinic acetylcholine receptor [abstract]. *J Nucl Med.* 2017;58:546.
36. Nabulsi N, Holden D, Zheng M-Q, et al. Evaluation of a novel, selective M1 muscarinic acetylcholine receptor ligand ^{11}C-LSN3172176 in non-human primates [abstract]. *J Nucl Med.* 2017;58:275.
37. Takai K, Sumiyoshi T, Suwa A, Takahashi Y, Uruno Y, Mura-Ta Y, Takashima H, inventors; Dainippon Sumitomo Pharma Co., LTD, Osaka, Japan, assignee. Fused-ring pyrrolidine derivative. WO2012020813A1 February 16, 2012.
38. Mogg AJ, Eessalu T, Johnson M, et al. In vitro pharmacological characterization and in vivo validation of LSN3172176 a novel M1 selective muscarinic receptor agonist tracer molecule for positron emission tomography. *J Pharmacol Exp Ther.* 2018;365:602–613.
39. Nabulsi NB, Mercier J, Holden D, et al. Synthesis and preclinical evaluation of ^{11}C-UCB-J as a PET tracer for imaging the synaptic vesicle glycoprotein 2A in the brain. *J Nucl Med.* 2016;57:777–784.
40. Sandiego CM, Weinzimmer D, Carson RE. Optimization of PET-MR registrations for nonhuman primates using mutual information measures: a multi-transform method (MTM). *Neuroimage.* 2013;64:571–581.
41. Hilton J, Yokoi F, Dannals RF, Ravert HT, Szabo Z, Wong DF. Column-switching HPLC for the analysis of plasma in PET imaging studies. *Nucl Med Biol.* 2000;27:627–630.
42. Wilson AA, Jin L, Garcia A, DaSilva JN, Houle S. An admonition when measuring the lipophilicity of radiotracers using counting techniques. *Appl Radiat Isot.* 2001;54:203–208.
43. Ichise M, Toyama H, Innis RB, Carson RE. Strategies to improve neuroreceptor parameter estimation by linear regression analysis. *J Cereb Blood Flow Metab.* 2002;22:1271–1281.
44. Innis RB, Cunningham VJ, Delforge J, et al. Consensus nomenclature for in vivo imaging of reversibly binding radioligands. *J Cereb Blood Flow Metab.* 2007; 27:1533–1539.
45. Lammertsma AA, Hume SP. Simplified reference tissue model for PET receptor studies. *Neuroimage.* 1996;4:153–158.

46. Cunningham VJ, Rabiner EA, Slifstein M, Laruelle M, Gunn RN. Measuring drug occupancy in the absence of a reference region: the Lassen plot re-visited. *J Cereb Blood Flow Metab.* 2010;30:46–50.
47. Larsen P, Ulin J, Dahlstrøm K, Jensen M. Synthesis of [^{11}C]iodomethane by iodination of [^{11}C]methane. *Appl Radiat Isot.* 1997;48:153–157.
48. Andersson Y, Cheng AP, Langstrom B. Palladium-promoted coupling reactions of [^{11}C]methyl iodide with organotin and organoboron compounds. *Acta Chem Scand.* 1995;49:683–688.
49. Suzuki M, Doi H, Koyama H, et al. Pd0-mediated rapid cross-coupling reactions, the rapid C-[^{11}C]methylations, revolutionarily advancing the syntheses of short-lived PET molecular probes. *Chem Rec.* 2014;14:516–541.
50. Waterhouse RN. Determination of lipophilicity and its use as a predictor of blood-brain barrier penetration of molecular imaging agents. *Mol Imaging Biol.* 2003;5:376–389.
51. Enna SJ, Bennett JP Jr, Bylund DB, et al. Neurotransmitter receptor binding: regional distribution in human brain. *J Neurochem.* 1977;28:233–236.
52. Mash DC, Potter LT. Autoradiographic localization of M1 and M2 muscarine receptors in the rat brain. *Neuroscience.* 1986;19:551–564.
53. Cortés R, Probst A, Tobler HJ, Palacios JM. Muscarinic cholinergic receptor subtypes in the human brain. II. Quantitative autoradiographic studies. *Brain Res.* 1986;362:239–253.
54. Bromberg-Martin ES, Matsumoto M, Hikosaka O. Dopamine in motivational control: rewarding, aversive, and alerting. *Neuron.* 2010;68:815–834.
55. Rinaldi A, Oliverio A, Mele A. Spatial memory, plasticity and nucleus accumbens. *Rev Neurosci.* 2012;23:527–541.
56. Parsey RV, Slifstein M, Hwang DR, et al. Validation and reproducibility of measurement of 5-HT1A receptor parameters with [carbonyl-^{11}C]WAY-100635 in humans: comparison of arterial and reference tissue input functions. *J Cereb Blood Flow Metab.* 2000;20:1111–1133.
57. Barth V, Need A. Identifying novel radiotracers for PET imaging of the brain: application of LC-MS/MS to tracer identification. *ACS Chem Neurosci.* 2014;5:1148–1153.
58. Need A, Kant N, Jesudason C, Barth V. Approaches for the discovery of novel positron emission tomography radiotracers for brain imaging. *Clin Transl Imaging.* 2017;5:265–274.
59. Jesudason CD, DuBois S, Johnson M, Barth VN, Need AB. In vivo receptor occupancy in rodents by LC-MS/MS. In: Sittampalam GS, Coussens NP, Brimacombe K, et al., eds. Assay Guidance Manual. Bethesda, MD; 2004: 955.
60. Yamamura HI, Kuhar MJ, Greenberg D, Snyder SH. Muscarinic cholinergic receptor binding: regional distribution in monkey brain. *Brain Res.* 1974;66:541–546.